Title
Hybrid Solar Cells based on Gallium Arsenide Nanopillars

Author
Haddad, Michael Anthony

Publication Date
2014

Peer reviewed|Thesis/dissertation

UNIVERSITY OF CALIFORNIA

Los Angeles

Hybrid Solar Cells Based on Gallium Arsenide Nanopillars

A thesis submitted in partial satisfaction

of the requirements for the degree Master of Science

in Electrical Engineering

by

Michael Anthony Haddad

2014

ABSTRACT OF THE THESIS

Hybrid Solar Cells Based on Gallium Arsenide Nanopillars

by

Michael Anthony Haddad

Master of Science in Electrical Engineering

University of California, Los Angeles, 2014

Professor Diana L. Huffaker, Chair

This thesis investigates the theory, fabrication, and characterization of nanostructured hybrid solar cells. Motivation for a hybrid organic-inorganic approach to solar cells is detailed and the benefits of nanopillars as an ideal framework for hybrid cells overviewed. The growth of selective area catalyst-free gallium arsenide nanopillars using metal organic chemical vapor deposition is discussed in detail. Next the step-by-step fabrication of the nanopillar growth mask and the hybrid solar cell device are overviewed. A main concern during fabrication is the uniform and sufficient coverage of the polymer on the nanopillar sidewalls. Multiple spin coatings of polymer are applied to the GaAs nanopillars to find an optimal polymer coating. Electrical characterization of the current-voltage characteristics under light and dark along with photocurrent over the UV-Visible spectrum is presented.

This thesis of Michael Anthony Haddad is approved.

Diana L. Huffaker, Committee Chair

Jia-Ming Liu

Kang Lung Wang

University of California, Los Angeles

2014

Table of Contents

1. Introduction **1**

2. Semiconductor Nanopillars: Growth and Applications **2**

2.1 Epitaxial Growth of III-V Nanopillars by MOVPE 2

2.2 Advantages of Selective Area Epitaxy 3

2.3 Growth of GaAs Nanopillars by MOCVD 4

3. Solar Cell Overview **6**

3.1 Hybrid Solar Cells 7

3.2 Exciton Harvesting 8

4. Nanopillar Hybrid Solar Cells **9**

4.1 Motivation and Prior Work 10

4.2 Design of PBnDT-FTAZ/GaAs Nanopillar Hybrid Solar Cell 13

4.3 Fabrication 15

4.4 Characterization 17

5. Summary **20**

References **22**

1. Introduction

This thesis covers the epitaxial growth of nanopillar arrays and their application in a hybrid organic-inorganic solar cell. First is an overview of the nanowire field and some of the potential applications. The differences between gold-catalyzed and self-catalyzed nanowire growth and the catalyst-free selective area epitaxy used to grow nanopillars are highlighted. The patterning of a gallium arsenide (GaAs) wafer with silicon dioxide and the associated lithography steps are overviewed. This patterning process is essential to forming an ordered array of uniform nanopillars. Next the growth conditions for a gallium arsenide nanopillar array grown by metal organic chemical vapor deposition are discussed in detail.

Motivation for a nanostructured hybrid solar cell is provided by reviewing the solar spectrum and discussing the advantageous properties of both semiconducting polymers and inorganic semiconductors. The hybrid organic-inorganic nanopillar solar cell device design is proposed and the fabrication steps detailed. Electrical characterization of the solar cell as well as transmission electron microscopy are presented and some conclusions are drawn about the quality of the junction that results. Some of the challenges associated with this device and potential improvements are considered in the summary.

2. Semiconductor Nanopillars: Growth and Applications

2.1 Epitaxial Growth of III-V Nanopillars by MOVPE

The growth in nanowire publications since the mid 1990s has been exponential, reaching almost 6000 related publications in 2009 [1]. Nanowires are created by epitaxy in both MOCVD and MBE [2], etched with reactive ion etching [3], and laser ablation [4]. The development of techniques to create nanowires is still growing today and these reviews provide an excellent overview [5-8]. Nanopillars can be considered a specific subset of nanowires. The growth mode discussed here is catalyst-free selective area epitaxy, and detailed in the figure below. It should be noted that certain nanopillar growth modes can be self-catalyzed, but that is not the case for Gallium Arsenide (GaAs) nanopillars. This is confirmed by the fact that growth can be interrupted and reinitiated without an appreciable change in growth rate and faceting. Also, there is no presence of a gallium droplet on top of the pillars for a variety of V/III growth conditions.

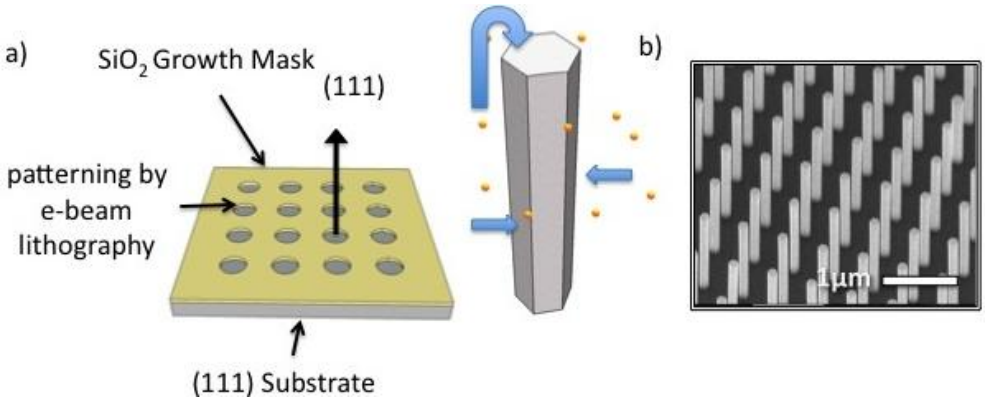

Figure 1 Schematic detailing the premise of selective area epitaxy **(a)** Surface preparation to grow vertical nanopillars. A (111) surface of either column III or V termination is required to form all vertical nanopillars. This substrate is then coated with a thin layer of SiO_2 and patterned with electron beam lithography. **(b)** Image of an array of GaAs pillars taken by a scanning electron microscope.

2.2 Advantages of Selective Area Epitaxy

Selective area epitaxy of nanopillars allows for precise control over nanopillar spacing, diameter, and pattern geometry. This level of control is achieved through electron beam patterning and is shown in the figure below. Large area patterning on a 4" wafer was demonstrated by deep ultraviolet (DUV) lithography. Our group has also demonstrated large area patterning through nanoimprint lithography.

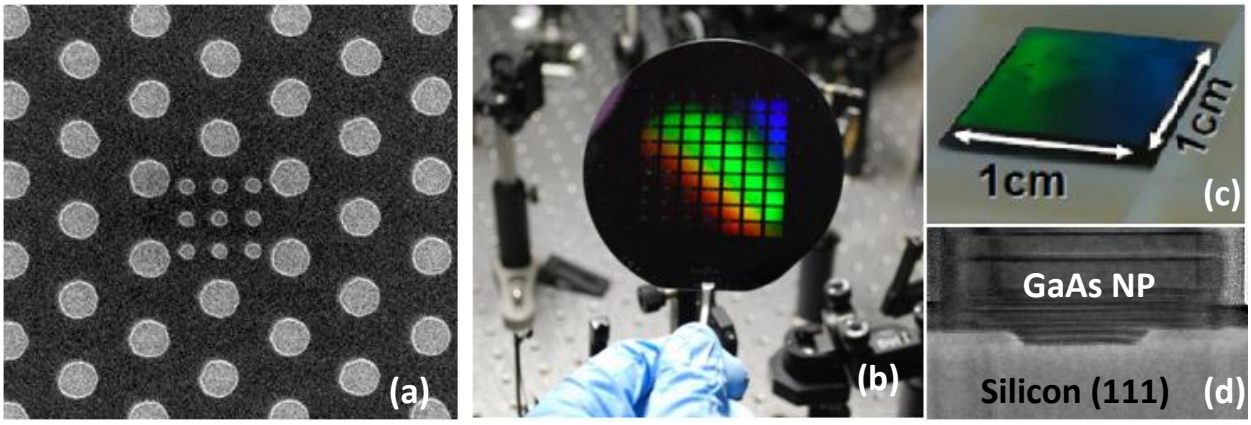

Figure 2 Outline of the patterning technologies available for nanopillar growth (a) Control over diameter, spacing, and pattern geometry by electron beam lithography. (b) Deep ultraviolet lithography on a 4" wafer. (c) Nanoimprint lithography used to create a GaAs nanopillar array on a 1 cm by 1 cm GaAs(111)B die. (d) Tunneling electron microscope image of the interface between Silicon(111) and a GaAs nanopillar.

The lines seen in the GaAs NP (**Figure 2d**) are due to stacking faults, commonly observed in GaAs NPs. However, the interface is defect free. The growth of III-V semiconductors on inexpensive Si(111) wafers provides an opportunity to integrate optoelectronic devices onto the same package as the well established silicon device processes. Even if a particular nanopillar is not grown on silicon, we have demonstrated the ability to peel off the nanopillars in a polymer resin and then reuse the substrate for pillar growth. The precise control over nanopillar dimensions and array layout has created a variety of uses for III-V nanopillars, both established devices with new properties or novel devices altogether.

The vertical arrays of nanopillars grown by our group have been used for plasmonically enhanced avalanche photo detectors [9], optically pumped photonic crystal lasers [10, 11], and solar cells [12]. Additionally, the pillars can be knocked down and placed onto oxide to form metal-oxide semiconductor field-effect transistors (MOSFETs). MOSFET models can be used to estimate carrier mobilities in the nanopillars and study the effect of surface states by comparing passivated and unpassivated nanopillar transistors [13].

2.3 Growth of GaAs Nanopillars by MOCVD

While there are many types of III-V semiconductors grown by selective area epitaxy, the focus here will be to overview the specific growth conditions for GaAs nanopillars. The GaAs nanopillars are used as the inorganic part of the hybrid solar cell devices discussed in Section 4. Nanopillars are grown by metal organic chemical vapor deposition (MOCVD) in a vertical, cold wall, Emcore Discovery 125 system (Emcore is now owned by Veeco). The carrier gas is hydrogen gas and only metal organics are used as precursors. The arsenic is sourced by tertiarybutylarsine (TBA), gallium sourced by trimethylgallium (TMGa), and n-type dopant sourced by triethyltin (TESn). Arsine is not used as a arsenic source due to concerns over

toxicity. It is important to note that the use of TBA makes the growth much more expensive and limits some growth techniques in the interest of material savings.

Growth is performed at a chamber pressure of 60 torr and a platter spin speed of 500 RPM. Material quantities entering the reactor are precisely controlled by digital readouts from pressure controllers and mass flow controllers with material quantities measured in $\mu mol/min$. While planar growth is often performed with an excess of the column V present at the surface, incorporating with the relatively sparse column III as favorable, nanopillar growth has proven to be more sensitive to the magnitude of column V present at the growth surface. Both the column III and V adatoms must be carefully controlled at the site of nucleation as well as the sidewalls of the nanopillar to promote vertical growth [14]. Nanopillars are in general grown at higher temperatures than the planar equivalents. GaAs has a relatively wide range of temperatures where vertical growth exceeds lateral growth and the temperature used here is 730°C.

Molar flow rates of TBA entering the reactor are 97 $\mu mol/min$ and TMGa of 8.6 $\mu mol/min$. The TESn has to be routed through a dilution network to achieve a molar flow on the order of 1E-5 to 1E-6 $\mu mol/min$. Since our MOCVD system did not have any available dilution networks attached to a metal organic source I installed additional stainless steel lines to route the metal organic through the rarely used disilane dilution network. The resulting function of this custom built dilution network is identical to the other dilution networks on the system.

With the conditions described above the nanopillars are grown for about ten to fifteen minutes to produce pillars with a 1 μm height. The height is sensitive to the diameter of the opening in the SiO_2 mask as well as the spacing between the pillars. The electron beam patterning used for the solar cell devices creates 60 nanometer hole sizes and 600 nanometer

pitch on a square pattern. The amount of dopants introduced into the pillars can also cause lateral overgrowth depending on the surfactant effect of the dopant. While ramping up to the growth temperature and ramping down, an arsenic overpressure is kept in the reactor to prevent arsenic desorption from both the substrate and nanopillar surfaces.

3. Solar Cell Overview

Solar cells have the unique ability to **directly** convert sunlight into electricity at a high conversion efficiency. Sunlight is radiative energy emitted by the sun due to a nuclear fusion reaction. The first solar cell was developed in 1954 and was a diffused silicon p-n junction [15]. Before considering the design and properties of a solar cell it is critical to understand the nature of solar radiation. The intensity of solar radiation in free space at the average distance of Earth from the sun is known as the solar constant (Solar Constant = 1353 W/m^2). While I will not cover the basic operation of a solar cell here, I will highlight the distribution of solar energy since it is one of the main motivations behind the hybrid solar cell discussed.

The solar constant is far from what is actually measured at sea level after sunlight has passed through the Earth's atmosphere. While accounting for the distance light travels through the Earth's atmosphere, it is necessary to quantify the average radiation per unit area. The average radiation per unit area is known as the radiative flux and is often referred to as irradiance. This average value is known as AM1.5 (AM1.5 = 844 W/m^2) which stands for air mass of 1.5 (Sun at 45° above the horizon). The sunlight at the top of the atmosphere is very similar to that of a black body radiator at 5525K (black line on the spectrum). Once you consider the absorption lines from water and carbon dioxide, and factor in Rayleigh scattering, you have a spectrum which resembles the irradiance at sea level, as shown in the figure below.

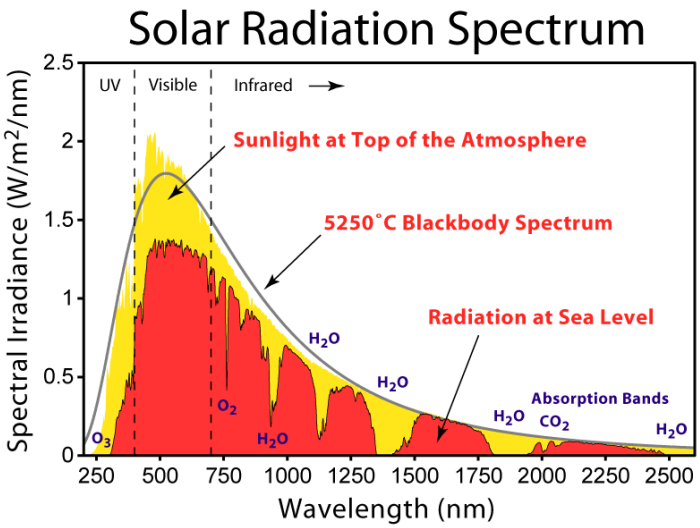

Figure 3 Solar radiation spectrum for direct light at the top of Earth's atmosphere and sea level. The large power density found near the UV-Vis range is readily absorbed by organic polymers.

Semiconductors from the III-Vs have a wide variety of band gap energies and exhibit both direct and indirect transitions. Whether or not a material has a direct or indirect transition strongly influences the end design of a solar cell. While both band gap alignments are useful for solar cells, the direct band gap alignment allows for the use of less material and smaller cells which leads to higher quantum efficiencies. In this thesis the focus will be on direct organic and inorganic semiconductors.

3.1 Hybrid Solar Cells

A hybrid solar cell is designed to take advantage of the high absorption coefficient and wide band gap found in organic materials, while utilizing the high electron mobility and relatively narrow band gap in inorganic materials. This configuration therefore calls for the inorganic to be the electron acceptor and the organic to be the electron donor. Polymer cells suffer from low mobilities for both electrons and holes, whereas most III-V semiconductors excel in transporting electrons. By combining the two materials there is potential to absorb a wider range of solar

irradiance while having half of the solar cell junction comprised of inexpensive organic polymer.

Due to the large absorption coefficient of organic polymers, ~10^6, standard polymer cells are able to be designed on the order of 1 micron. Despite the 1 micron width of a polymer cell there is still considerable series resistance found in these cells and often the shunt resistance of the cell is poor as well, degrading the fill factor of the device. Another key difference when considering photon absorption in an organic is that the photon does not simply excite an electron to the valence band, which is then free to propagate under the influence drift and/or diffusion. Absorbed photons in a polymer generate excitons that have an even lower mobility than electrons and holes. An exciton is the bound state of an electron and a hole due to the Coulomb force. The average exciton diffusion length in a semiconducting polymer is on the order of 10 to 20 nanometers [16]. While exciton disassociation is not fully understood at organic interfaces, it is accepted that the exciton must reach a boundary between the hole and electron acceptor.

3.2 Exciton Harvesting

There are two mechanisms to generate unbound electrons and holes at the donor-acceptor junction. The first is electron transfer by exciton diffusion in close proximity of an interface (tens of nanometers). Once the exciton is near the junction an electron will move into the conduction band-tail of the inorganic, benefiting from the high electron mobility of the inorganic and reducing the probability of recombination prior to extraction of the separated charge carrier. In the energy transfer mechanism the exciton moves into the inorganic prior to a hole being transferred to the organic semiconductor. Based on the valence band-HOMO (Highest Occupied Molecular Orbital) offset this mechanism is more energetically favorable as the energy of the HOMO level increases relative to the valence band-tail. The end result of both processes is a

separation of charge carriers. Tuning the band alignment between the inorganic and organic materials is critical for achieving an efficient charge carrier separation rate.

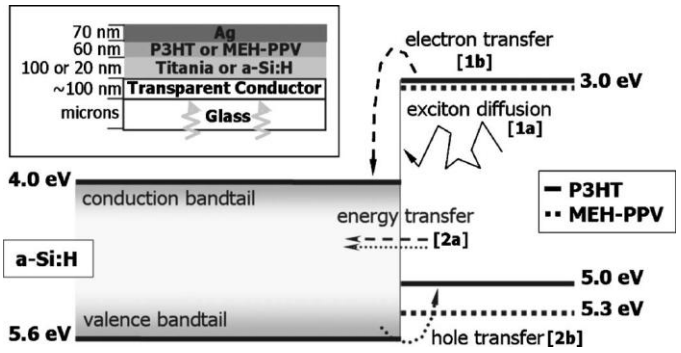

Figure 4 The cell configuration is shown in the top left corner. The two mechanisms of exciton harvesting are shown. (1a) exciton diffusion followed by (1b) electron transfer. (2a) energy transfer followed by (2b) hole transfer [17]

Mechanism 1 is enhanced by large exciton diffusion lengths and a favorable offset between the polymer LUMO (Lowest Unoccupied Molecular Orbital) and the inorganic conduction band. Tuning these two parameters is key to improving efficiency for hybrid solar cells dominated by this mechanism of carrier generation.

Mechanism 2 is enhanced by exciton diffusion lengths and a favorable offset between the HOMO of the organic and the valence band of the inorganic. This is known as backward hole transfer efficiency [17, 18]. To fully characterize a hybrid solar cell it is necessary to identify the dominant exciton harvesting mechanism and look for ways to improve it. As always, looking to improve exciton diffusion length within the bulk will increase collection efficiency.

4. Nanopillar Hybrid Solar Cells

4.1 Motivation and Prior Work

Neugebauer et al. proposed that the ideal structure of a bulk heterojunction polymer solar cell is a well ordered donor and acceptor phase interspaced with an average length of 10 to 20 nanometers [19].

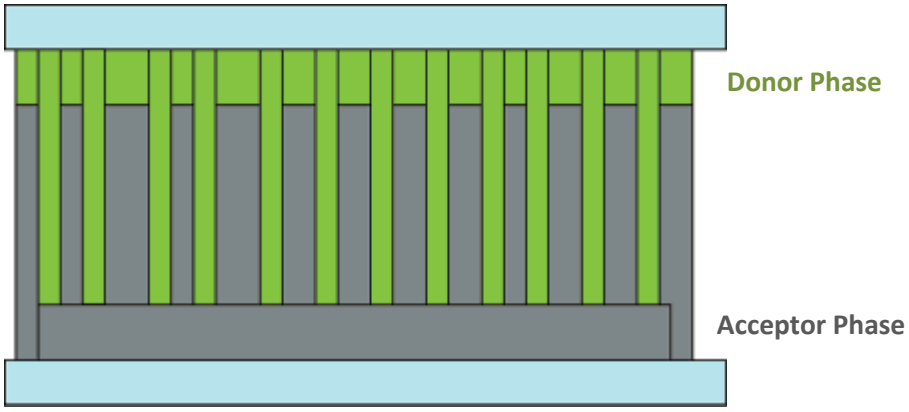

Figure 5 The ideal structure of a bulk heterojunction solar cell. The acceptor and donor phases are interspaced with an average spacing of 10-20 nm (approximately the exciton diffusion length) [19].

Since progress to create materials with increased exciton diffusion lengths has been slow, a conjugated polymer matrix that has boundaries on the nanometer scale is of interest. In addition to providing an ideal spacing for exciton disassociation, the inorganic-organic matrix creates ideal channels for charge carriers to be separated to their respective electrodes.

Prior work on hybrid solar cells has traditionally looked to reduce the number of fabrication steps involved in semiconductor fabrication. Ion implantation is a common technique to form a p-n junction for a silicon based device. While ion implantation followed by a rapid thermal anneal is not an expensive technique relative to other semiconductor fabrication steps, it is still significantly more expensive and slower than a spin coating process involving an organic polymer. Nanostructured hybrid devices have been demonstrated achieving a power conversion efficiency over 9.7% [20]. Shen, Sun et al. have used silicon nanowires are created by a wet-etch

process from an amorphous p-type silicon layer as a nanowire array. This array is then coated with PEDOT:PSS to form a Schottky solar cell, since PEDOT:PSS is not an absorber but rather an organic and transparent conductor. An array of reactive ion etched (RIE) GaAs nanowires highlights the effectiveness of interpenetrating GaAs as an electron pathway. Planar GaAs/PEDOT:PSS cells exhibited efficiencies of 0.29% while the GaAs nanowire array exhibited efficiencies of 5.8% [21].

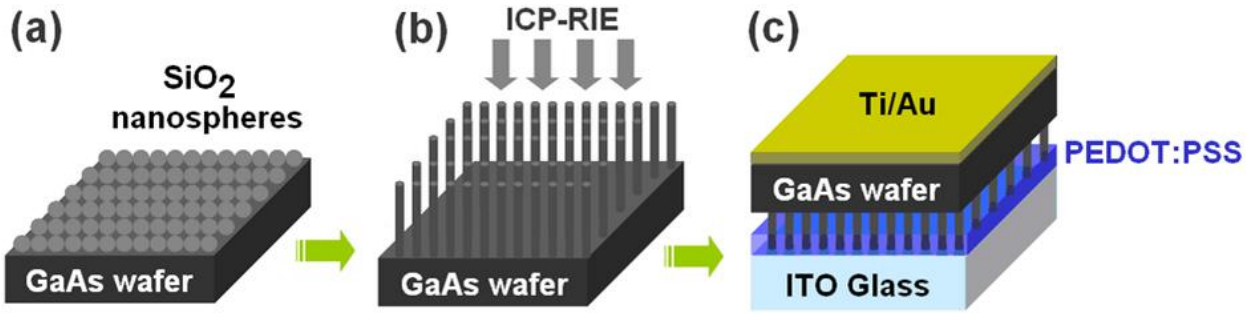

Figure 6 The steps in fabricating GaAs NW/PEDOT:PSS hybrid solar cells. (a) Spinning a monolayer of SiO_2 nanospheres as the etch mask. (b) Dry-etching to fabricate GaAs NW arrays with the inductively coupled plasma reactive ion etching system, and (c) attaching GaAs NW arrays onto the PEDOT:PSS conductive polymer layer coated on ITO glass [21].

An alternative approach is to use a semiconducting organic polymer. This approach is more complex and the physics of the organic-inorganic interface are poorly understood. Device efficiencies have traditionally been below that of the hybrid Schottky cells, but the potential of such devices due to the increased range of absorption presents an interesting research avenue. A GaAs/poly(3-hexylthiophene (P3HT, medium band gap polymer) hybrid nanostructured device has a reported efficiency under 1% [22]. Similar InP/P3HT hybrid nanostructured devices also reported efficiencies under 1% [23]. The figure below shows the band alignment for a GaAs/P3HT device.

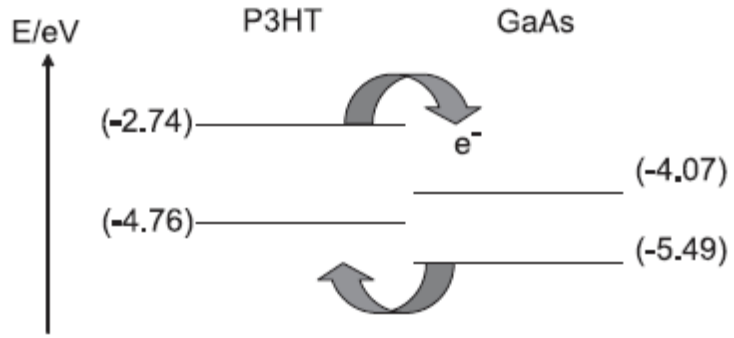

Figure 7 Band alignment for a hybrid solar cell of P3HT and Gallium Arsenide.

P3HT is currently the mid band gap polymer of choice for solar applications. One of the most efficient and common organic solar cells consists of P3HT:PCBM (phenyl C_{61}-butyric acid methyl ester). The power conversion efficiency of these cells is between 4 and 5% [24]. The high-lying HOMO level of P3HT will effectively limit the open circuit voltage of a solar cell and subsequently limit the efficiency of the cell. Development of medium band gap polymers with lower lying HOMO levels has been of interest to increase efficiency. PBnDT-FTAZ, a fluorinated polymer with a medium band gap, showed efficiencies over 7% when blended with PCBM [25]. The hole mobility of PBnDT-FTAZ is also higher than P3HT which will increase the incident photon to current efficiency. The next section will overview the design and fabrication of a PBnDT-FTAZ/GaAs nanopillar hybrid solar cell.

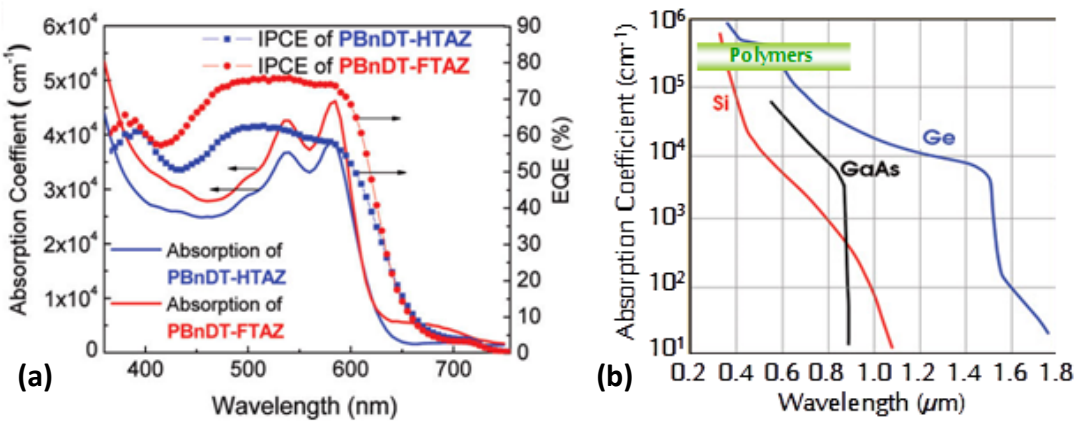

Figure 8 **(a)** Incident photon to current efficiency and solid film absorption of each blend of polymer:$PC_{61}BM$ [25] **(b)** Absorption coefficients for Silicon (Si), Gallium Arsenide (GaAs), Germanium (Ge), and the general range for polymers in the ultraviolet to visible region (UV-vis).

4.2 Design of PBnDT-FTAZ/GaAs Nanopillar Hybrid Solar Cell

As discussed in the previous section, patterned nanopillar arrays provide close to the ideal matrix for a hybrid solar cell. To increase the IPCE of the hybrid cell above that of a planar configuration a cell design approaching this ideal case is created. A thin layer of organic polymer, on the order of the exciton diffusion length, can be applied uniformly to the large surface area of the three-dimensional pillar array. In this configuration, the polymer is able to absorb incident light despite being very thin. This is possible due to the high absorption coefficient, as discussed in the previous sections, and the increased optical path length provided by nanopillar arrays [26].

As seen in Figure 9, the HOMO-level of FTAZ closely matches the valence band of GaAs. It is thought that this will help promote exciton transfer from the FTAZ to the GaAs (Mechanism 2 for exciton harvesting). As described in the prior work, hybrid solar cells designed with a semiconducting polymer show low efficiency and often times an S-kink in the fourth

quadrant of the I-V curve under light. The S-kink seen in the I-V curves has been attributed to strong interface dipoles measured by ultraviolet photoelectron spectroscopy. [27].

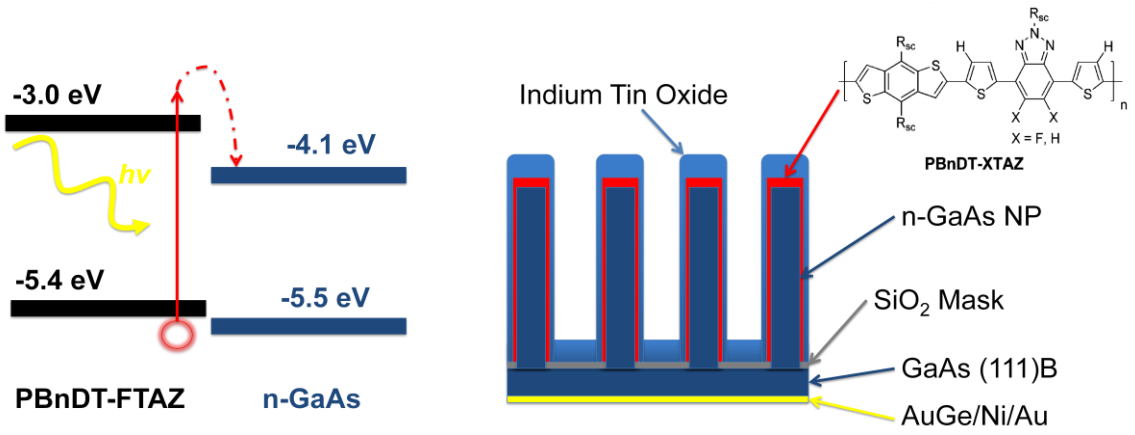

Figure 9 Proposed hybrid organic-inorganic band alignment. The nanostructured hybrid solar cell is defined by the spacing, height, and diameter of the nanopillars.

Surface states are also a large concern for all nanowires, with the concern magnified for an organic-inorganic interface. Surface passivation using ammonium hydroxide has been shown to provide a substantial reduction in surface state density in nanowires [13]. Octanethiol was investigated as a passivating agent as well, but the octanethiol interfered with the adhesion of the polymer to the GaAs nanopillars. The adhesion of the polymer was unaffected by ammonium hydroxide and the design below was fabricated with and without the surface passivation.

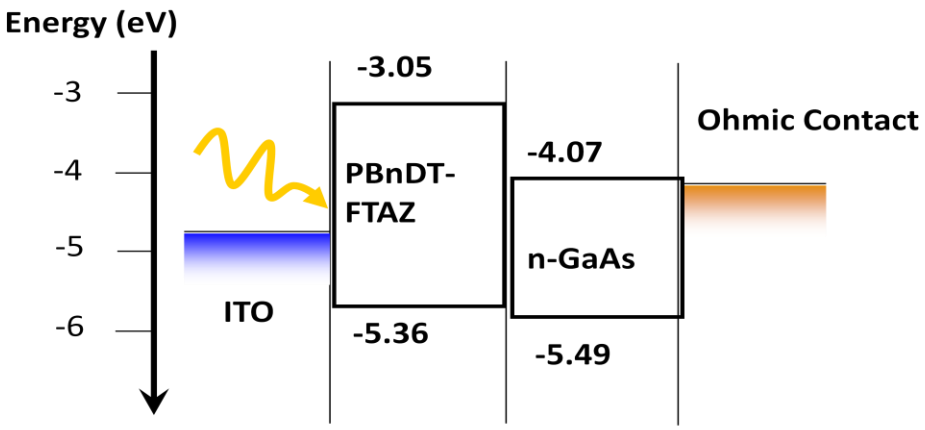

Figure 10 Detailed band alignment of the PBnDT-FTAZ and the n-type Gallium Arsenide. Careful consideration of the metal electrodes is required to extract carriers efficiently. Electrons are transferred to the n-GaAs nanopillar and extracted through the AuGe/Ni/Au contact. Holes are extracted through the Indium Tin Oxide (ITO) contact.

4.3 Fabrication

Patterned arrays of GaAs nanopillars are epitaxially grown on a 1 cm by 1 cm die as described in the previous section on epitaxial growth. On each die there are 4 square patches measuring 500 μm. Within the 500 μm patch the pitch between each pillar is 600 nm in a square lattice. The openings in the SiO_2 mask are approximately 80 nm after the reactive ion etch to expose the substrate. With tin doping the diameter of 1 micron tall nanopillars is approximately 90-100 nm.

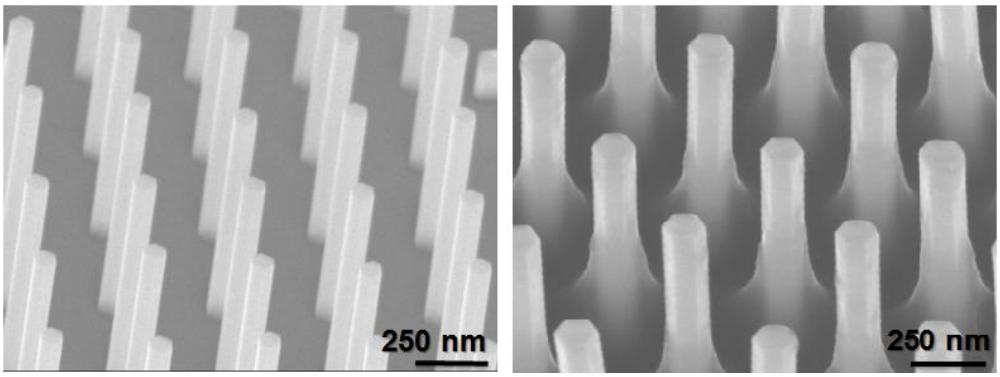

Figure 11 **(a)** As-grown nanopillar array of Gallium Arsenide. The pitch between each pillar is 600nm while the nanopillar height is approximately 1 $\boldsymbol{\mu m}$ and the diameter is approximately 100 nm. **(b)** 10 mg/mL polymer solution (PBnDT-FTAZ) in trichlorobenzene is spin coated at 1000 RPM.

Multiple spin coats have been shown to increase the thickness of the polymer surrounding the pillar and increase the photocurrent.

Figure 11b shows the array after a spin coating of PBnDT-FTAZ. The polymer was provided by the You group (University of North Carolina, Chapel Hill) in solid form. The polymer was weighed and diluted with trichlorobenzene at several different dilutions. The polymer was then heated at 80°C overnight and kept away from light and under vacuum in a dessicator. The spin coating was done on a standard nitrogen purged spin coater at several different RPMs. The polymer was applied to the sample using a static dispense. Polymer dilution and spin speed were two major factors controlling the adhesion of the polymer to the nanopillar and whether or not the polymer could infiltrate the voids between pillars. Additionally, letting the polymer settle with no rotation for up to a minute helped to promote infiltration and adhesion to the nanopillars. If the polymer was not dilute enough the voids would not be filled. Excessive dilution led to insufficient adhesion of the polymer to the nanopillar sidewalls. Ultimately the spin coating process is not ideal for coating the nanopillar side and top facets. The process is complicated by the different surface energies exhibited by the different crystal orientations and the general issue of infiltration when the pitch is under one micron. If the coating is too thick then the excitons cannot reach the organic-inorganic interface to be harvested. On the other hand if the coating is too thin then the junction becomes a Schottky cell comprised of GaAs and indium tin oxide. Spin coating on planar surfaces is a successful technique to reproduce thin uniform films, but on nanostructures other techniques may be more effective. Electrodeposition has demonstrated conformal coating of nanopillars with control over the width of the coating and the dopant type [12].

After many combinations of dilution, spin speed, and other phyiscal manipulations, a thin coating of polymer was observed over the array of nanopillars. Figure 12 shows a cross sectional SEM of the polymer coating with an indium tin oxide (ITO) transparent top contact. Depositing ITO onto the polymer requires careful ramping of the deposition power to prevent heating of the polymer which can lead to cracking.

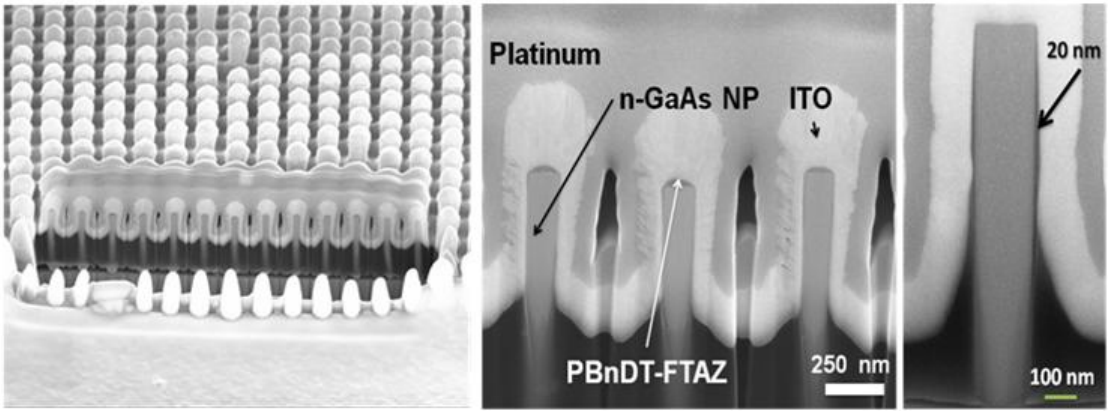

Figure 12 Cross-sectional SEM of the nanopillar array shown in the previous figure. Platinum is deposited on top of the area to be cut, protecting the sample from the damaging focused ion beam.

The large volume of polymer towards the bottom of the array is significant for device performance. The high absorption coefficient coupled with the low exciton diffusion length means that any light that does not get absorbed before reaching this large volume of polymer does not contribute to the photocurrent. Ideally, the polymer would be uniform around the pillar with no excess polymer settling along the SiO_2 mask.

4.4 Characterization

Immediately after processing the devices were measured for light and dark current-voltage characteristics and photoresponse. Two separate sets of devices that were fabricated and characterized are covered in this section. The hybrid solar cell light I-V was characterized using the simulated AM 1.5 light source shown in Figure 13.

Figure 13 Experimental setup for I-V measurements. For measurements, the beam from the xenon lamp (a) is reflected through the mirror at (d) onto the sample stage at (e). The lamp includes a shutter located at (b) which also houses a filter to simulate the AM1.5 peaks. Probes located at (f) and (g) are used for the top-top contacting scheme used in the devices measured.

The photoresponse was measured from 400 nm to 1 um using a white light source sent through a grating spectrometer and then passed through a filter wheel outputting a 1 mm beam that overfilled the device area.

The I-V and EQE in Figure 14 represent the first attempt at fabrication for the hybrid solar cell. It was difficult to prove the existence of a thin polymer layer via trasmission electron microscopy. At this stage in the project dilution of the polymer with trichlorobenzene was not fully optimized and it is thought that most of the polymer was actually at the GaAs substrate. The GaAs substrate is covered in SiO_2 and any polymer at the bottom of the pillars is much thicker (similar to Figure 12, without the coating around the pillar) than the exciton diffusion length.

The figures of merit for the I-V curve indicate that the device is more likely a Schottky diode formed between n-GaAs and ITO. The properties of the dark I-V curves suggest this conclusion along with published data for a planar GaAs/ITO junction [28]. The ideality factor was measured to be 1.4 with a series resistance of approximately 140 Ω and a rectification ratio of 10^4 measured at one volt. Under light the fill factor was very similar to a planar GaAs/ITO

(sputtered) cell in terms of both open circuit voltage (0.46 V) and fill factor (57%). All of this suggests that further optimization was needed for the polymer dilution to ensure a conformal polymer coating on the nanopillar sidewalls.

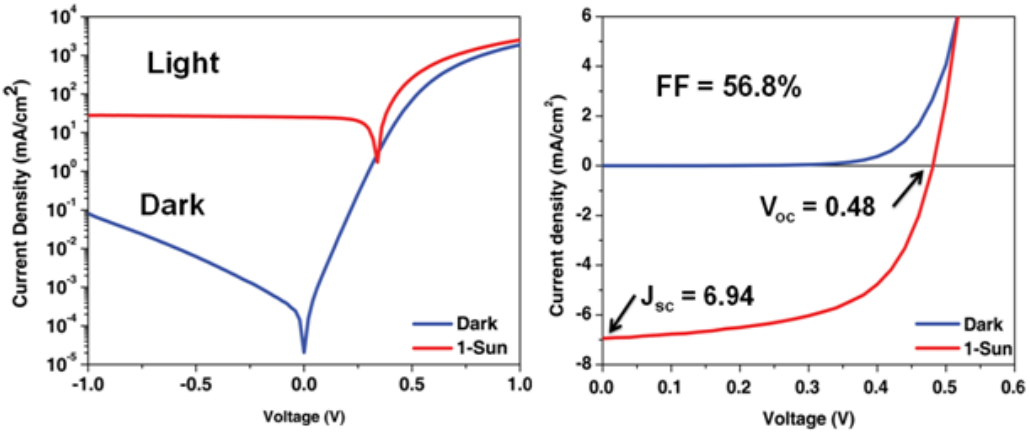

Figure 14 (a) Semi-log current-voltage (I-V) plot of the hybrid cells under no illumination and 1-Sun illumination. **(b)** Linear plot of the I-V highlighting the short circuit current density, open circuit voltage, and the fill factor.

The next experiment was designed to study the effect of multiple PBnDT-FTAZ coatings. Such an experiment would help to ensure a sufficient coating to avoid the GaAs/ITO junction seen in the last experiment while also tuning the polymer thickness to maximize absorption. The results of this experiment for one, two, and three polymer coatings are shown in Figure 15. Upon initial inspection there is evidence of an S-kink described previously [27]. While the S-kink has an overall negative impact on the solar cell performance by decreasing the fill factor, it is a strong indicator that the junction formed for these devices is indeed between the GaAs/PBnDT-FTAZ and not the GaAs/ITO. The presence of an S-kink could be attributed to the interface dipoles created between the {110} sidewall facets of the nanopillar and the PBnDT-FTAZ. The formation of such a surface dipole between the various facets of GaAs and conjugated polymers

is poorly understood and requires modeling of the interface to extend the understanding beyond experimental observation.

While the overall solar cell performance is inferior to the GaAs/ITO cell, it is interesting to note that the highest short circuit current and open circuit voltage are observed for two spin coatings of PBnDT-FTAZ. This could be attributed to the strong dependence of hybrid solar cell performance on polymer thickness. Two spin coatings could be providing sufficient thickness to maximize absorption by the polymer while simultaneously minimizing the exciton travel distance to reach the heterointerface and contribute to the photocurrent.

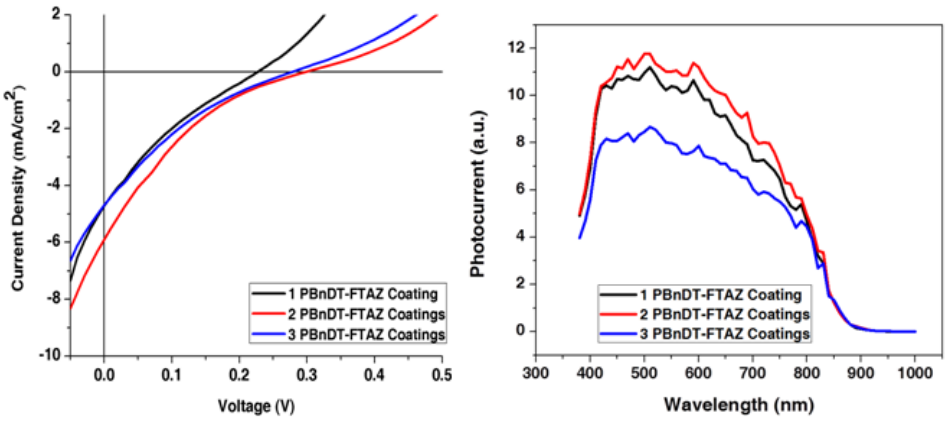

Figure 15 (a) Linear I-V plot for one, two, and three spin coatings of PBnDT-FTAZ. The highest current density and open circuit voltage are observed for **two** spin coatings of PBnDT-FTAZ. **(b)** Associated photocurrent measurement for one, two, and three spin coatings of PBnDT-FTAZ.

5. Summary

The fabrication of a nanostructured hybrid solar cell has been demonstrated. Catalyst-free selective area epitaxy of GaAs nanopillars formed the inorganic section of the solar cell. The polymer PBnDT-FTAZ has been spin coated with one, two, and three coatings to form the organic portion of the junction. The devices showed that the polymer dilution must be carefully controlled and applied to ensure that the junction is formed between the polymer and GaAs nanopillar and not the GaAs and ITO. Two spin coatings show a marginal improvement over one and three spin coatings. The variability in the spin

coating process and difficulty in controlling the polymer on the nanopillar sidewalls suggests that other techniques may be preferable for the fabrication of this device. The S-kink observed under light suggests that further study of the interface is required to determine if the interface states seen between GaAs {110} and PBnDT-FTAZ can be mitigated. Different polymers could be investigated to see if the performance improves. Additionally a hole transfer layer could help alleviate the S-kink condition. Ultimately the GaAs interface between semiconducting polymers remains unexplored and further study is required to better understand the exciton collection and overall cell performance.

References

1. Yang, P., R. Yan, and M. Fardy, *Semiconductor Nanowire: What's Next?* Nano Letters, 2010. **10**(5): p. 1529-1536.

2. Wu, Y. and P. Yang, *Direct observation of vapor-liquid-solid nanowire growth.* JOURNAL-AMERICAN CHEMICAL SOCIETY, 2001. **123**(13): p. 3165-3166.

3. Chou, S.Y., P.R. Krauss, and P.J. Renstrom, *Imprint of sub-25 nm vias and trenches in polymers.* Applied Physics Letters, 1995. **67**: p. 3114.

4. Morales, A.M. and C.M. Lieber, *A laser ablation method for the synthesis of crystalline semiconductor nanowires.* Science, 1998. **279**(5348): p. 208-211.

5. Schmidt, V., et al., *Silicon Nanowires: A Review on Aspects of their Growth and their Electrical Properties.* Advanced Materials, 2009. **21**(25-26): p. 2681-2702.

6. Gao, Q., et al., *Growth and properties of III–V compound semiconductor heterostructure nanowires.* Semiconductor Science and Technology, 2011. **26**(1): p. 014035.

7. Johansson, J. and K.A. Dick, *Recent advances in semiconductor nanowire heterostructures.* CrystEngComm, 2011. **13**(24): p. 7175-7184.

8. Mårtensson, T., et al., *Epitaxial III-V nanowires on silicon.* Nano Letters, 2004. **4**(10): p. 1987-1990.

9. Senanayake, P., et al., *Photoconductive gain in patterned nanopillar photodetector arrays.* Applied Physics Letters, 2010. **97**(20): p. 203108-3.

10. Scofield, A., et al. *Bottom-up photonic crystal cavities formed by III-V nanopillar arrays*. 2011. Optical Society of America.

11. Scofield, A., et al. *Room Temperature Continuous Wave Lasing in Nanopillar Photonic Crystal Cavities*. 2012. Optical Society of America.

12. Mariani, G., et al., *Three-Dimensional Core–Shell Hybrid Solar Cells via Controlled in Situ Materials Engineering.* Nano Letters, 2012. **12**(7): p. 3581-3586.

13. Andrew, L., et al., *Extracting transport parameters in GaAs nanopillars grown by selective-area epitaxy.* Nanotechnology, 2012. **23**(10): p. 105701.

14. Björk, M.T., et al., *InAs nanowire growth on oxide-masked 〈111〉 silicon.* Journal of Crystal Growth, 2012. **344**(1): p. 31-37.

15. Chapin, D.M., C.S. Fuller, and G.L. Pearson, *A New Silicon p-n Junction Photocell for Converting Solar Radiation into Electrical Power.* Journal of Applied Physics, 1954. **25**(5): p. 676-677.

16. Nunzi, J.-M., *Organic photovoltaic materials and devices.* Comptes Rendus Physique, 2002. **3**(4): p. 523-542.

17. Gowrishankar, V., et al., *Exciton harvesting, charge transfer, and charge-carrier transport in amorphous-silicon nanopillar/polymer hybrid solar cells.* Journal of Applied Physics, 2008. **103**(6): p. 064511-8.

18. Gowrishankar, V., et al., *Exciton splitting and carrier transport across the amorphous-silicon/polymer solar cell interface.* Applied Physics Letters, 2006. **89**(25): p. 252102-3.

19. Günes, S., H. Neugebauer, and N.S. Sariciftci, *Conjugated Polymer-Based Organic Solar Cells.* Chemical Reviews, 2007. **107**(4): p. 1324-1338.

20. Shen, X., et al., *Hybrid Heterojunction Solar Cell Based on Organic–Inorganic Silicon Nanowire Array Architecture.* Journal of the American Chemical Society, 2011. **133**(48): p. 19408-19415.

21. Jiun-Jie, C., et al., *GaAs nanowire/poly(3,4-ethylenedioxythiophene):poly(styrenesulfonate) hybrid solar cells.* Nanotechnology, 2010. **21**(28): p. 285203.

22. Bi, H. and R.R. LaPierre, *A GaAs nanowire/P3HT hybrid photovoltaic device.* Nanotechnology, 2009. **20**(46): p. 465205.

23. Novotny, C.J., E.T. Yu, and P.K.L. Yu, *InP Nanowire/Polymer Hybrid Photodiode.* Nano Letters, 2008. **8**(3): p. 775-779.

24. Ma, W., et al., *Thermally Stable, Efficient Polymer Solar Cells with Nanoscale Control of the Interpenetrating Network Morphology.* Advanced Functional Materials, 2005. **15**(10): p. 1617-1622.

25. Price, S.C., et al., *Fluorine Substituted Conjugated Polymer of Medium Band Gap Yields 7% Efficiency in Polymer–Fullerene Solar Cells.* Journal of the American Chemical Society, 2011. **133**(12): p. 4625-4631.

26. Mariani, G., et al., *Hybrid conjugated polymer solar cells using patterned GaAs nanopillars.* Applied Physics Letters, 2010. **97**(1): p. 013107-3.

27. Kumar, A., S. Sista, and Y. Yang, *Dipole induced anomalous S-shape I-V curves in polymer solar cells.* Journal of Applied Physics, 2009. **105**(9): p. 094512-6.

28. Sheldon, P., et al., *Evaluation of ITO/GaAs solar cells.* Journal of Vacuum Science and Technology, 1982. **20**(3): p. 410-413.